This behavior is readily observed during the alignment of cells and collagen fibers in directions of maximum tensile stresses [5–7] and maximum effective stiffness. A key to understand these phenomena resides in our ability to characterize how cells interact with their environment and especially how they are able to sense their mechanical surrounding and react by producing contractile

overall deformation has been addressed in a previous study [15]. We show here that this feature can be naturally coupled with a model for SF remodeling to capture realistic cell behaviors. At last, the level set method is ideal to model phenomena such as growth and evolution [24], which are inherent in cell spreading and remodeling. The present framework, although not addressing the problem of growth, is an important stepping stone to engaging in such study in the future.

The organization of the paper is as follows. In the next section, we give a summary of the constrained mixture model to characterize cell contraction; we particularly concentrate on providing the main equations (conservation of mass and momentum) as well as a set of biologically relevant assumptions to build realistic constitutive relations. In Section 3, the problem of the interaction between a cell and a deformable substrate is investigated. Governing equations are derived in both their strong and weak form, which enables a smooth transition to the finite element formulation presented in Section 4. Section 4 then discusses the XFEM–level set approach to obtain a solution of the cell–substrate interactions, leading to the final form of implicit, time-dependent finite element equations. The method is then illustrated in Section 5 by presenting several experimentally motivated example of cell–substrate interactions with comparison to observations. The paper finishes with a brief summary and concluding remarks.

2. A CONSTRAINED MIXTURE MODEL OF CONTRACTILE CELLS

2.1. Continuum description of cell's structure

The mechanosensing capability of cells is closely related to their contractile abilities. The latter has mainly been explained in terms of the formation of a well-differentiated network of SFs that are capable of generating forces through actomyosin interactions [14, 25, 26]. The main processes behind cell contraction can generally be decomposed as follows: first, the assembly of SF from dissolved contractile units and second, the contractile capacity of SFs. On the one hand, SF assembly and dissociation are known to be very sensitive to mechanical stimuli; mechanical force stabilizes existing SFs and promotes the assembly of new ones [26]. On the other hand, the contractile capacity of SFs is regulated by cross-bridge dynamics, which is known to be very sensitive to strain and strain rate. The evolution of SF therefore depends on the ability of cells to sense and transmit mechanical force from the substrate through so-called focal adhesion complexes (Figure 5) [27]. These complexes provide a physical attachment between SFs and substrate-anchoring molecules (ligands) through cross-membrane proteins (integrins) and may be thought of as cohesion islands of finite size between cell and substrate [28, 29]. At last, the internal structure of fibroblasts possesses sub-membranous mechanical reinforcement, known as the cortex, which is found in the form of a thin layer of actin fibers oriented in parallel with the membrane [9, 30–32]. This component is known to have a significant effect on the cell's morphology and deformation by providing a non-negligible tangential stiffness to the cell membrane [15].

From a modeling perspective, cell and substrate can be defined by two physical domains ^{c} and ^{s} in their current configuration, whose boundaries are denoted by ^{c} and ^{s}, respectively (Figure 1). Whereas a substrate is modeled as a purely elastic medium, a contractile cell is viewed

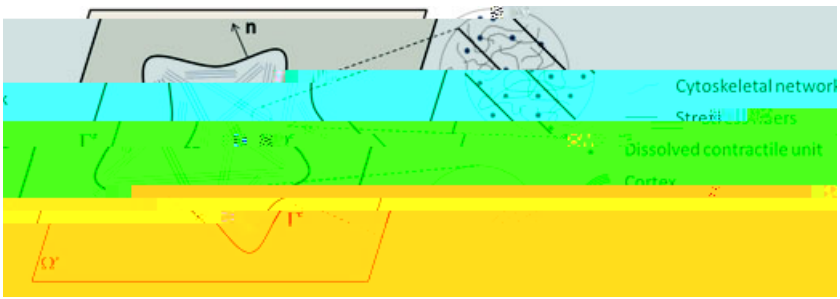

Figure 1. A typical cell on a substrate: the definition of domains and boundaries and a cell's main constituents.

DOI: 10.1002/nme

as a constrained mixture made of four constituents [14] (Figure 1): two solid constituents, a passive cytoskeleton (mostly made of microtubules and intermediate filaments) and a highly anisotropic SF network, and two fluid components, the cytosol and a population of dissolved contractile units. Measuring material motion with respect to the passive cytoskeleton, for which a point in the original configuration is denoted by $\mathbf{X}$, we can give a description of the mixture at any time in terms of respective volume fraction ϕ^α of the diverse constituents. Considering a saturated mixture, it can further be shown that the summation of all volume fractions at a point is equal to 1, that is, $\sum_{\alpha=1}^{4} \phi^\alpha(\mathbf{X}, \cdot) = 1$, where $\alpha = \mathrm{s, f, m, p}$ for passive cytoskeleton, cytosol, dissolved contractile units, and SFs, respectively. When placed on elastic substrates, fibroblasts usually evolve quickly in a configuration in which their thickness is significantly smaller than other dimensions, which motivates our study within the context of two-dimensional plane stress assumptions. This generally simplifies the analysis as SF directions only occupy the two-dimensional space and can be described in terms of one orientation angle. At any point within the cell, the SF network may then be defined in terms of the so-called structure tensor $\mathbf{\Phi}^{\mathrm{p}}$ given by [14]

$$\mathbf{\Phi}^{\mathrm{p}}(\mathbf{X}, \cdot) = \phi^{\mathrm{p}} \left[\eta \mathbf{I} + (1 - \eta)\, \mathbf{M}_{\theta_0} \right], \qquad \mathbf{M}_{\theta_0} = \begin{bmatrix} \cos^2\theta_0 & \cos\theta_0 \sin\theta_0 \\ \cos\theta_0 \sin\theta_0 & \sin^2\theta_0 \end{bmatrix}, \tag{1}$$

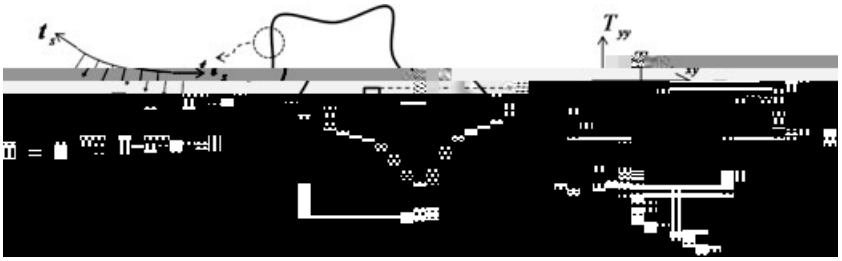

Figure 2. Equilibrium of forces in the body and the boundary of a cell.

2.3. Balance of momentum

Let us now turn to the governing equation describing the equilibrium of forces within a cell (Figure 2). For this, it is of interest to define the mixture Cauchy stress tensor **T** representing the infinitesimal force per unit current area. Using the effective stress principle, we can decompose the mixture stress into a contribution from each constituent,

$$\mathbf{T} \mathrm{D} \mathbf{T}^{c} \mathrm{C} \mathbf{T}^{p} \quad \mathbf{I}, \tag{7}$$

where $\mathbf{T}^{c}$ is the partial stress in the passive cytoskeleton, $\mathbf{T}^{p}$ is the stress that originates from the presence of SFs, and is the fluid pressure. Note that the contribution from the pressure of dissolved contractile proteins has been neglected because of its relatively low volume fraction. Considering the balance of momentum for the mixture, we can derive the form

$$\mathrm{r} \quad \mathbf{T} \mathrm{C} \mathbf{b} \mathrm{D} \mathbf{0} \quad \text{in} \quad {}^{c}, \tag{8}$$

representing the balance of force within the cell domain. Note that dynamical effects (through the inertial term) were neglected because of the slow processes into consideration. Finally, we note that by invoking the balance of angular momentum, we can show that stresses $\mathbf{T}^{c}$, $\mathbf{T}^{p}$

Here, κ denotes the isotropic permeability of the cytoskeleton and μ is the viscosity of the cytosol. Note that because of the appearance of SF, the permeability may become anisotropic in time. This effect is not accounted for in the present study. In addition, we assume that the motion of dissolved proteins is driven by two forces: (1) the drag force of the cytosol and (2) the diffusive forces through the cytosol. One can therefore show that the flux $\mathbf{J}^{m}$ of proteins contains a convection and diffusion term,

$$\mathbf{J}^{m} = \frac{\phi^{m}}{\phi^{f}} \frac{\kappa}{\mu} \nabla \qquad \phi^{f} \quad \nabla \left(\frac{\phi^{m}}{\phi^{f}} \right), \tag{11}$$

where is the diffusion coefficient of dissolved proteins in the cytosol.

To characterize the elasticity of the passive cytoskeleton, a hypo-elastic constitutive relation

their contribution in each direction. Assuming that the normalized uniaxial stress in a specific direction is given by the product of functions and , weighted by their volume fraction ϕ^{p}, the stress $\mathbf{T}^{p}$ is defined by

$$\mathbf{T}^{\mathrm{p}} \mathrm{D} \frac{\hat{T}}{\pi} \int_{-\pi/2}^{\pi/2} \phi^{\mathrm{p}}\ \theta \quad \mathrm{p} \quad \begin{matrix} \cos^2\theta & \cos\theta\sin\theta \\ \cos\theta\sin\theta & \sin^2\theta \end{matrix} \quad \mathrm{d}\theta, \tag{19}$$

where is related to the Green–Lagrange strain tensor $\mathbf{E}$ by $\mathrm{D}\ \hat{E}_{11}\cos^2\theta\ \mathrm{C}\ \hat{E}_{22}\sin^2\theta\ \mathrm{C}\ \hat{E}_{12}\sin\theta\ \cos\theta$ and the quantity $\hat{T}$ denotes the typical magnitude of SF isometric contraction in fibroblasts. Note that the value of ϕ^{p} for different directions is determined from the knowledge of the structure's tensor $\mathbf{\Phi}^{\mathrm{p}}$ as described in [14].

A particularity of the preceding model of cell contraction is that it generates a positive feedback mechanism between fiber contraction and formation in the direction in which fiber shortening is mostly resisted. For instance, when cells adhere to a stiff substrate, their contraction only generates little deformation, which according to the tension–velocity curve enables SF to keep a level of isometric contraction. The presence of such a contraction consequently promotes more SF formation in this particular direction as described by the mechanosensitive formation model of (16). Inversely, a cell adhering to a soft substrate generates a significant amount of negative strains as a result of contraction. This results in switching the strain rate to the left of the tension–velocity curve in Figure 4 and thus decreasing the magnitude of SF contraction. Ultimately, this is translated into a drop in the rate of fiber formation and a loss of SF density.

3. GOVERNING EQUATIONS FOR THE CELL–SUBSTRATE INTERACTION PROBLEM

We now turn to the formulation of the interactions between cells and their mechanical environment. We particularly concentrate on the problem of cells lying on a two-dimensional elastic substrate, a situation that often arises both *in vivo* and in experiments.

3.1. Substrate elasticity

The mechanical behavior of the substrate is known to be an important factor driving cell morphology, contraction, and structure [27, 31, 39–41]. Although this behavior can be extremely complex, involving nonlinear elasticity, viscous effects, and inelasticity, the present work concentrates on the case of a simple linear isotropic elastic material with varying stiffness. Describing substrate deformation in terms of a displacement field $\mathbf{u}^{\mathrm{s}}$, one can introduce a rate of deformation and an objective rate for the substrate Cauchy stress $\mathbf{T}^{\mathrm{s}}$ in a similar form as that shown in (12). In other words, substrate elasticity is described in terms of two parameters (λ^{s}, μ^{s}) or equivalently by the set (, ν^{s}) denoting Young's modulus and Poisson's ratio, respectively. It is finally straightforward to show that substrate equilibrium is written in terms of the divergence of the Cauchy stress as

$$\mathrm{r}\quad \mathbf{T}^{\mathrm{s}} \mathrm{C}\ \mathbf{b}^{\mathrm{s}} \mathrm{D}\ \mathbf{0}, \tag{20}$$

where $\mathbf{b}^{\mathrm{s}}$ represents the body force vector in the substrate. In the following analysis, we assume that the substrate consists of a very thin layer that can be modeled in plane stress conditions. Although this situation may not accurately represent actual experimental conditions, the assumption is not expected to affect the main trends exhibited by cell in terms of different substrate elasticities.

3.2. Adhesion complexes

Cell–substrate adhesion is provided by the attachment between transmembrane molecules (known as integrins) and molecular complex (the ligands) lying on the surface of the substrate (Figure 5). Integrins easily diffuse through the cell membrane [42] to attach to free ligands on the substrate. It is thus realistic to assume that the magnitude of the adhesive force $\mathbf{t}_{\mathrm{a}}$ per unit area is directly related to the density η_{l} of ligands on the substrate by

$$\mathbf{t}_{\mathrm{a}} \mathrm{D}\ \eta_{\mathrm{l}}\mathbf{f}_{\mathrm{a}}, \tag{21}$$

DOI: 10.1002/nme

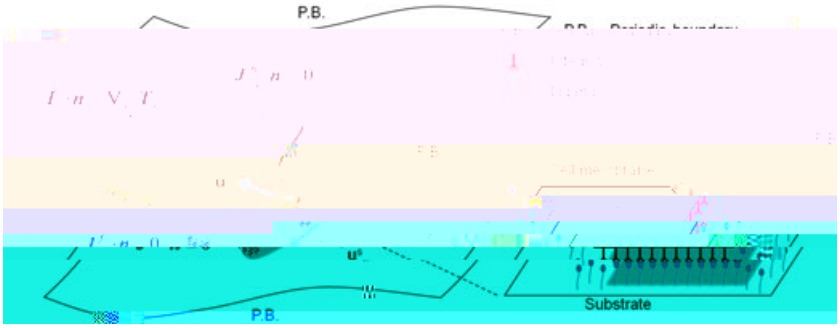

Figure 5. The general details of adhesion complexes between cell and substrate combined of integrins and ligands; together with the boundary conditions applied to cell and substrate.

where η_l denotes the number of ligands per unit substrate area and $\mathbf{f}_a$ is the force in a single ligand–integrin complex. Further assuming that the mechanical behavior of a ligand–integrin complex is represented by a linear force–separation relation with stiffness $_{li}$, the continuum traction force (per unit area) is given by

$$\mathbf{t}_a \mathrm{D} \quad _a \ \mathbf{u}^c \quad \mathbf{u}^s \ , \quad \text{where} \quad _a \mathrm{D} \ \eta_l \ _{li}, \tag{22}$$

where the term $\mathbf{u}^c \quad \mathbf{u}^s$ represents the separation between the cell membrane and the substrate surface. The preceding equation clearly states the stiffness of the adhesion stiffness increases linearly with ligand density. It also shows that if no ligands are present $\eta_l \mathrm{D}$, no cell–substrate adhesion is possible ($\mathbf{t}_a \mathrm{D}$).

3.3. Summary of the governing equations under plane stress conditions: strong form

Considering that the cell and the substrate lie in the – plane of the (, , ,) -coordinate system, plane stress conditions imply that stress components associated with the , -direction vanish. In addition, adhesion forces $\mathbf{t}_{a}$

In the end, the five equations ((23), (24), (25), (26), and (27)) subjected to the given boundary conditions can be solved to determine five unknowns that consist of the following: (1) the displacement field $\mathbf{u}^{s}\ \mathbf{X},$ in the substrate domain ^{s}; (2) the displacement field $\mathbf{u}\ \mathbf{X},$ in the cell domain ^{c}; (3) the cytosol volume fraction $\phi^{f}\ \mathbf{X},$ in ^{c}; (4) the monomer volume fraction $\phi^{m}\ \mathbf{X},$ in ^{c}; and finally, (5) the structure tensor $\mathbf{\Phi}^{p}\ \mathbf{X},$ describing the SF distribution in ^{c}.

3.4. Summary of the governing equations: weak form

The earlier coupled differential equations constitute a highly nonlinear system whose solution lies in the three-dimensional space , , . A numerical strategy based on the FEM is therefore necessary to obtain a solution in the most general case. Such a formulation requires that governing equations are rewritten in an integral form (or weak form) as described in this section. For this, we introduce arbitrary admissible weighting functions denoted by scalars functions θ and λ, vector functions $\boldsymbol{\omega}$ and $\boldsymbol{\omega}^{s}$, and a second-order tensor function $\mathbf{\Lambda}$. Multiplying each governing equation ((23), (24), (25), (26), and (27)) with a corresponding weight function and integrating over their associated domain, we obtain five scalar equations as follows:

$$\int_{\Omega^{s}} \boldsymbol{\omega}^{s}$$

4. LEVEL SET–EXTENDED FEM FORMULATION

4.1. Numerical strategy for cell–substrate interactions

From a numerical viewpoint, the cell–substrate interaction under plane stress assumptions involves two superposed domains ^{s} and ^{c}, of arbitrary shapes, on which different, but interacting, fields must be computed (Figure 1). To solve such a problem, two strategies may be adopted. The first would consist in introducing different discretizations for each domain, on which solutions would be computed separately but can interact through a numerical treatment of the interactions at cell–substrate adhesions. The second, introduced in this paper, only requires a single discretization, used for both cell and substrate. In this approach, whereas the substrate domain ^{s} is entirely contained in the computational domain, the cell domain ^{c} is defined in terms of a level set function that defines the arbitrary contour of the cell.

Referring to Figure 6a, the level set function $\phi\ \mathbf{X}$ is a function of space (in the undeformed configuration) that is represented by a two-dimensional surface in a three-dimensional space. The two-dimensional morphology of the cell is then defined as the intersection of this surface with the $-$ plane of the cell (Figure 6a). The function ϕ is chosen such that its sign is opposite in two sides of the cell boundary, which enables a clear definition concerning the location of material point P located at $\mathbf{X}$ with respect to the cell domain:

$$\text{if } \phi\ \mathbf{X} \quad , \quad 2 \quad ^{c}, \tag{38}$$

$$\text{if } \phi\ \mathbf{X}\ \mathrm{D}\ , \quad 2 \quad ^{c}, \tag{39}$$

$$\text{if } \phi\ \mathbf{X} \quad , \quad \ldots \quad ^{c}. \tag{40}$$

In addition, the level set function enables the definition of the unit vector $\mathbf{n}_0$ that is normal to the cell boundary ^{c} in its original configuration,

$$\mathbf{n}_0\ \mathbf{X}\ \mathrm{D}\ \frac{\mathrm{r}_{\mathbf{X}}\phi\ \mathbf{X}}{\mathrm{jj}\,\mathrm{r}_{\mathbf{X}}\phi\ \mathbf{X}\,\mathrm{jj}}, \tag{41}$$

where $\mathrm{r}_{\mathbf{X}}$ denotes the gradient with respect to the initial coordinate $\mathbf{X}$ and jj jj denotes the $_2$ norm. This strategy enables us to define arbitrary cell morphologies independently from finite element discretization. Furthermore, nodes located outside of the cell domain are only associated with substrate displacement $\mathbf{u}^{s}$ whereas nodes that are located in ^{c}

morphologies. In numerical simulations, this leads to significant issues with meshing, especially when three-dimensional shapes are considered. The presented method circumvents this issue by defining a shape geometry using a mesh-independent level set function. We note that

The function $\mathbf{x})$ is used to introduce a jump in the fields $\mathbf{u}^{c}$, p, ϕ^{m}, and $\mathbf{\Phi}^{p}$ across the cell's membrane, whereas the ridge function is used to define discontinuities in their spatial derivative [21, 50]. A one-dimensional representation of the Heaviside and ridge functions is provided in Figure 6b and c

4.3. Discretization and time integration

The linearized finite element equation is obtained by substituting the XFEM approximation (42) corresponding to each continuum field $\mathbf{u}^{s}$, $\mathbf{u}$, ϕ^{m}, and $\mathbf{\Phi}^{p}$ into the linearized weak-form equations

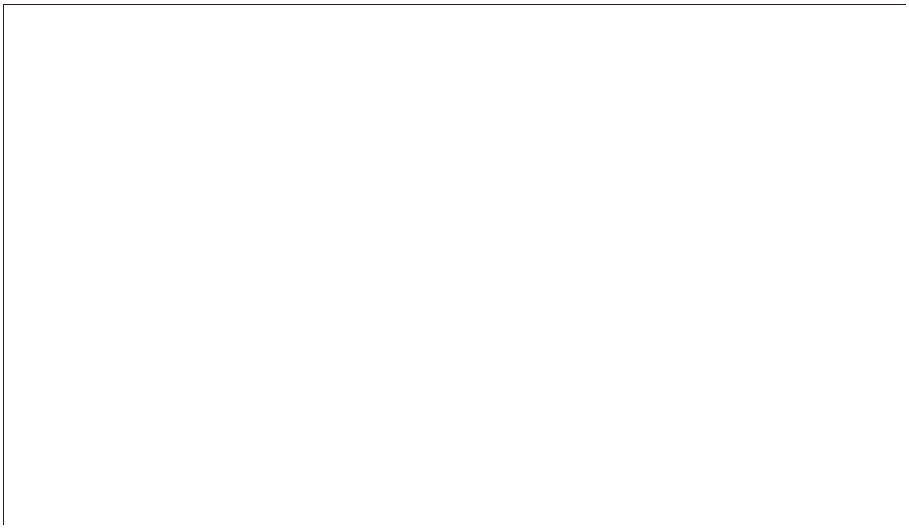

Table I. Parameters used in the simulations.

Definition	Symbol	Value	Unit	Reference
Cytosol volume fraction	ϕ^{c}	70	%	[53]
Cytoskeleton volume fraction	ϕ^{s}	25	%	n/a
F C G actin volume fraction	ϕ^{m} C ϕ^{p}	5	%	n/a
Rate of SF formation	$^{f}_{0}$	0.0001	s^{-1}	[54]
Mechanosensitive rate of SF formation	$^{f}_{1}$	0.05	s^{-1}	[54]
Rate of SF dissociation	$^{d}_{0}$	0.1	s^{-1}	[54]
Cytoskeleton permeability	κ μ	$^{-15}$	m^4 N s	[55]
G-actin diffusion constant		$^{-5}$	m^2 s	[54]
Young's modulus	$^{\blacksquare}_{2}$	70	Pa	[12]
Poisson's ratio	ν	.		[12]
Fiber maximum tensile stress	$^{N}_{f}$	20,000	Pa	[33, 56, 57]
Reference strain rate (Equation (17))	^{p}			

where the parameters μ D . and μ D . were obtained for the XFEM and the FEM, respectively, for D [58]. Note that the values of the parameter μ for the FEM and the XFEM are calculated for the same time step, and the lower value of μ for the XFEM indicates a better rate of convergence in comparison with FEM.

5.2. Effect of cell morphology on stress fiber development

As noted in the previous section, one main advantage of using the XFEM–level set approach relies in that cell geometry can be defined independently from discretization. In this example, we take advantage of this capability to investigate the SF evolution in three cells, characterized by different geometries (square, rectangle, and triangle) and substrate adhesion (Figure 10a–c) on an elastic substrate whose elastic modulus is 100 Pa. Because of their simple geometries, square and rectangular cells can easily be handled with the ordinary FEM; for validation purposes, we therefore compute solutions using both the XFEM and the FEM, when subjected to the same element size. In addition, although initial conditions are the same as in the previous section, we applied periodic boundary conditions on the substrate domain to simulate an infinitely large domain with a periodic cell's structure. More details on this approach are given in [59].

Figure 10d–f shows the first stress invariant in the substrates due to cell contraction at steady state. These results clearly show that compressive state of stress beneath the cell(v)15(-311.4(ehg15(1lath)enstah2dSgX

with experimental observations for similar conditions (the insets of Figure 10g–i) [60–63]. Here, our results show that SFs are preferably generated in directions of maximum apparent stiffness, corresponding to lines connecting adhesion islands. This can be explained as follows. In direc-

A relevant question in biology is to understand how the mechanical work performed by cells is

APPENDIX B: INCREMENTAL WEAK FORM OF THE GOVERNED EQUATIONS

Before writing the incremental form of the set of derived equations, we need to find equations for $\delta\phi^f$ and $\dot{\phi}^f$ D ϕ^f as a function of cell's variables. As mentioned before, cell's body is assumed to be saturated by four constituents: cytoskeletal network, cytosol, SF polymers, and G-actin monomers; consequently, one can write ϕ^f C ϕ^c C ϕ^p C ϕ^m D . After deriving the material time derivative of the latter equation, we obtain the formula $\dot{\phi}^f$ D $\dot{\phi}^c$ $\dot{\phi}^p$ $\dot{\phi}^m$, where ϕ denotes the volume fraction of each cell's component and the superscripts f, c, p, and m stand for cytosol, cytoskeleton, polymers, and monomers, respectively. Furthermore, following [14] and considering plane stress condition for the cell, the balance of mass equation for cytoskeleton takes the following form: ϕ^c D $\dot{\phi}^c$ D $\phi^c \alpha$ r $\dot{\mathbf{u}}$ $\phi^c \beta$ $\dot{p}$.

As a result,

$$\begin{aligned} \dot{\phi}^f &= \phi^c \alpha \, \mathrm{r} \cdot \dot{\mathbf{u}} + \phi^c \beta \, \dot{p} - \mathrm{tr}\left(\dot{\boldsymbol{\Phi}}^p\right) - \dot{\phi}^m \\ \delta\phi^f &= \phi^c \alpha \, \mathrm{r} \cdot \delta\mathbf{u} + \phi^c \beta \, \delta p - \mathrm{tr}\left(\delta\boldsymbol{\Phi}^p\right) - \delta\phi^m \end{aligned} \quad . \tag{B.1}$$

$$Z \quad \text{"}$$
$$\Lambda \; \mathbb{W} \quad \mathrm{p}$$
$$\Omega^{c}$$

Furthermore, the following definitions will be used for discretization:

$$\boldsymbol{\omega}^{s} \mathrm{D} \mathbf{N}^{s} \quad \boldsymbol{\omega}^{s,e} \mathrm{I} \quad \boldsymbol{\omega} \mathrm{D} \mathbf{N} \quad \boldsymbol{\omega}^{e} \mathrm{I} \quad \theta \mathrm{D} \mathbf{N}_{f} \quad \boldsymbol{\theta}^{e} \mathrm{I} \quad \lambda \mathrm{D} \mathbf{N}_{f} \quad \boldsymbol{\lambda}^{e} \mathrm{I} \quad \boldsymbol{\Lambda} \mathrm{D} \mathbf{N}_{p} \quad \boldsymbol{\Lambda}^{e}, \tag{C.8}$$

$$\mathbf{u}^{s} \mathrm{D} \mathbf{N}^{s} \quad \mathbf{u}^{s,e} \mathrm{I} \quad \mathbf{u} \mathrm{D} \mathbf{N} \quad \mathbf{u}^{e} \mathrm{I} \quad \mathrm{D} \mathbf{N}_{f} \quad \mathbf{p}^{e} \mathrm{I} \quad \phi^{m} \mathrm{D} \mathbf{N}_{f} \quad \boldsymbol{\Phi}^{m,e} \mathrm{I} \quad \boldsymbol{\Phi}^{p} \mathrm{D} \mathbf{N}_{p} \boldsymbol{\Phi}^{p,e}, \tag{C.9}$$

$$\mathrm{r} \boldsymbol{\omega}^{s} \mathrm{D} \mathbf{B}^{s} \quad \boldsymbol{\omega}^{s,e} \mathrm{I} \quad \mathrm{r} \boldsymbol{\omega} \mathrm{D} \mathbf{B} \quad \boldsymbol{\omega}^{e} \mathrm{I} \quad \mathrm{r} \theta \mathrm{D} \mathbf{B}_{f} \quad \boldsymbol{\theta}^{e} \mathrm{I} \quad \mathrm{r} \lambda \mathrm{D} \mathbf{B}_{f} \quad \boldsymbol{\lambda}^{e}, \tag{C.10}$$

$$\mathrm{r} \mathbf{u}^{s} \mathrm{D} \mathbf{B}^{s} \quad \mathbf{u}$$

$$\omega^{e\mathrm{T}} \int_{\Omega^{c,e}} \mathbf{B}^{\mathrm{T}} \left({}^{1}\hat{\mathbf{T}}^{\mathrm{co}} + {}^{1}\hat{\mathbf{T}}^{\mathrm{po}} + {}^{1}\mathbf{C}^{\mathrm{co}} \right) \mathbf{B}\, \delta\mathbf{u}^{e} + {}^{11}\mathbf{T}^{\mathrm{coo}}\, \mathbf{G}\, \delta\mathbf{u}^{e} + {}^{1}\mathbf{T}^{\mathrm{po}}$$

In the preceding equations, $\mathbf{m}^{\mathrm{T}} = \{1\ 1\ 0\}$, and the matrix $\mathbf{M}_{\mathrm{p}}$ is defined such that in Voigt notation one can write $\{\mathbf{A}_{\sigma}\} = \mathbf{M}_{\mathrm{p}}\{\mathbf{A}\}$, where $\{\mathbf{A}_{\sigma}\}$ and $\{\mathbf{A}\}$ are vector forms of symmetric tensors $\mathbf{A}_{\sigma}$ and $\mathbf{A}$, respectively. As a result, the matrix $\mathbf{M}_{\mathrm{p}}$ takes the following form [48]:

$$\mathbf{M}_{\mathrm{p}} = \begin{bmatrix} n_{11}^2 & n_{12}^2 & n_{11}n_{12} \\ n_{12}^2 & n_{22}^2 & n_{22}n_{12} \\ 2n_{11}n_{12} & 2n_{22}n_{12} & n_{12}^2 + n_{11}n_{22} \end{bmatrix}. \tag{C.25}$$

Also, the cortex's stiffness matrix $\{\mathbf{S}_{\sigma}\}$ can be calculated by using its elastic matrix $\{\mathbf{C}_{\sigma}\}$ by $\{\mathbf{S}_{\sigma}\} = \mathbf{M}_{\mathrm{p}}^{\mathrm{T}}\{\mathbf{C}_{\sigma}\}\mathbf{M}_{\mathrm{p}}$. Furthermore, the notation $\{\mathbf{C}\}$ is used to define the fourth-order constitutive matrix $\mathbf{C}$ as a second-order matrix in Voigt notation.

APPENDIX D: COMPONENTS OF FINAL EQUATION (46)

The components of Equation (46) are given by the following:

$$\mathbf{F}^{u^s,e} = \int_{\Omega^s} \mathbf{B}^{s\mathrm{T}}\{\hat{\boldsymbol{\tau}}^{s}\}\,d\Omega^{s} - \int_{\Omega^c} \mathbf{N}^{s\mathrm{T}}\{\hat{\mathbf{t}}_a\}\,d\Omega^{c}, \tag{D.1}$$

$$\mathbf{F}^{u,e} = \int_{\Omega^c} \left[\mathbf{B}^{\mathrm{T}}\{\hat{\boldsymbol{\tau}}^{c}\} + \{\hat{\boldsymbol{\tau}}^{p}\}\right]\mathbf{B}\,d\Omega^{c} + \int_{\Omega^c} \mathbf{N}^{\mathrm{T}}\{\hat{\mathbf{t}}_a\}\,d\Omega^{c} + \int_{\Omega^c} \mathbf{B}^{\mathrm{T}}\mathbf{M}_{\mathrm{p}}^{\mathrm{T}}\{\hat{\boldsymbol{\tau}}_{\sigma}\}\,d\Omega^{c}, \tag{D.2}$$

$$\mathbf{F}^{f,e} = \int_{\Omega^c} \mathbf{B}_{\mathrm{f}}^{\mathrm{T}}\left[\frac{\kappa}{\mu}\mathbf{B}_{\mathrm{f}}\,\mathbf{p}^{e} + \frac{\phi^{m}}{\phi}\right]

$$\mathbf{K}^{fu,e} = \int_{\Omega^c} \mathbf{B}_f^T \frac{\partial \phi^m}{\partial \phi^f} \left(\frac{\partial}{\partial \phi^f}\left(\frac{\kappa}{\mu}\mathbf{B}_f\right)\mathbf{p}^e + \frac{\partial}{\partial \phi^f}\left(-\mathbf{r}\phi^f + \phi^c \alpha \hat{\mathbf{B}}\right)\right) d\Omega^c - \int_{\Omega^c} \mathbf{B}_f^T \frac{\partial \phi^m}{\partial \phi^f} \left(\mathbf{B}\left(\phi^c \alpha \hat{\mathbf{B}}\right)\right) d\Omega^c, \tag{D.12}$$

$$\mathbf{K}^{ff,e} = \int_{\Omega^c} \mathbf{B}_f^T \left(\frac{\partial \phi^m}{\partial \phi^f}\frac{\kappa}{\mu}\mathbf{B}_f\right) d\Omega^c + \int_{\Omega^c} \mathbf{B}_f^T \frac{\partial \phi^m}{\partial \phi^f} \left(\frac{\partial}{\partial \phi^f}\left(\frac{\kappa}{\mu}\mathbf{B}_f\right)\mathbf{p}^e + \frac{\partial}{\partial \phi^f}\left(-\mathbf{r}\phi^f + \phi^c \beta \mathbf{N}_f\right)\right) d\Omega^c - \int_{\Omega^c} \mathbf{B}_f^T \frac{\partial \phi^m}{\partial \phi^f} \left(\mathbf{B}\left(\phi^c \beta \mathbf{N}_f\right)\right) d\Omega^c, \tag{D.13}$$

$$\mathbf{K}^{fm,e} = \int_{\Omega^c} \mathbf{B}_f^T \left(\frac{\partial}{\partial \phi^f}\left(\frac{\kappa}{\mu}\mathbf{B}_f\right)\mathbf{p}^e \mathbf{N}_f + \mathbf{B}_f \frac{\partial}{\partial \phi^f}\left(-\mathbf{r}\phi^f \mathbf{N}_f\right)\right) d\Omega^c + \int_{\Omega^c} \mathbf{B}_f^T \frac{\partial \phi^m}{\partial \phi^f} \left(\frac{\partial}{\partial \phi^f}\left(\frac{\kappa}{\mu}\mathbf{B}_f\right)\mathbf{p}^e + \frac{\partial}{\partial \phi^f}\left(-\mathbf{r}\phi^f\right)\mathbf{N}_f\right) d\Omega^c - \int_{\Omega^c} \mathbf{B}_f^T \frac{\partial \phi^m}{\partial \phi^f} \left(\mathbf{B}\,\mathbf{N}_f\right) d\Omega^c, \tag{D.14}$$

$$\mathbf{K}^{fp,e} = \int_{\Omega^c} \mathbf{B}_f^T \frac{\partial \phi^m}{\partial \phi^f} \left(\frac{\partial}{\partial \phi^f}\left(\frac{\kappa}{\mu}\mathbf{B}_f\right)\mathbf{p}^e + \frac{\partial}{\partial \phi^f}\left(-\mathbf{r}\phi^f\right)\mathbf{m}^T \mathbf{N}_p\right) d\Omega^c - \int_{\Omega^c} \mathbf{B}_f^T \frac{\partial \phi^m}{\partial \phi^f} \left(\mathbf{B}\,\mathbf{m}^T \mathbf{N}_p\right) d\Omega^c, \tag{D.15}$$

$$\mathbf{K}^{mf,e} = \int_{\Omega^c} \mathbf{B}_f^T \left(\frac{\kappa}{\mu}\mathbf{B}_f\right) d\Omega^c, \tag{D.16}$$

$$\mathbf{K}^{pu,e} = \int_{\Omega^c} \mathbf{N}_p^T \,m,$$

and

$$\mathbf{C}^{\mathrm{ff},e} = \int_{\Omega^c} \mathbf{N}_{\mathrm{f}}^{\mathrm{T}} \beta \mathbf{N}_{\mathrm{f}} \, \mathrm{d}\Omega^c, \tag{D.23}$$

$$\mathbf{C}^{\mathrm{m}u,e} = \int_{\Omega^c} \mathbf{N}_{\mathrm{f}}^{\mathrm{T}} \left(\phi^{\mathrm{c}} + \phi^{\mathrm{f}} \right) \alpha \hat{\mathbf{B}} \, \mathrm{d}\Omega^c, \tag{D.24}$$

$$\mathbf{C}^{\mathrm{mf},e} = \int_{\Omega^c} \mathbf{N}_{\mathrm{f}}^{\mathrm{T}} \left(\phi^{\mathrm{c}} + \phi^{\mathrm{f}} \right) \beta \mathbf{N}_{\mathrm{f}} \, \mathrm{d}\Omega^c, \tag{D.25}$$

$$\mathbf{C}^{\mathrm{mm},e} = \int_{\Omega^c} \mathbf{N}_{\mathrm{f}}^{\mathrm{T}} \mathbf{N}_{\mathrm{f}} \, \mathrm{d}\Omega^c, \tag{D.26}$$

$$\mathbf{C}^{\mathrm{mp},e} = \int_{\Omega^c} \mathbf{N}_{\mathrm{f}}^{\mathrm{T}} \mathbf{m}^{\mathrm{T}} \mathbf{N}_{\mathrm{p}} \, \mathrm{d}\Omega^c, \tag{D.27}$$

$$\mathbf{C}^{\mathrm{p}u,e} = \int_{\Omega^c} \left[\mathbf{N}_{\mathrm{p}}^{\mathrm{T}} {}^{1}\boldsymbol{\Phi}^{\mathrm{po}} \alpha \hat{\mathbf{B}} + \mathbf{N}_{\mathrm{p}}^{\mathrm{T}} \frac{\phi^{\mathrm{p}}}{\phi^{\mathrm{m}}} \frac{\phi^{\mathrm{f}}}{1} \frac{{}^{1}\mathbf{T}^{\mathrm{po}}}{{}^{1}\mathbf{E}^{\mathrm{po}}} \mathbf{F}^{\mathrm{m}} \mathbf{B} \frac{\partial \phi^{\mathrm{m}}}{\partial \phi^{\mathrm{f}}} \right] \mathrm{d}\Omega^c, \tag{D.28}$$

$$\mathbf{C}^{\mathrm{pf},e} = \int_{\Omega^c} \mathbf{N}_{\mathrm{p}}^{\mathrm{T}} {}^{1}\boldsymbol{\Phi}^{\mathrm{po}} \beta \mathbf{N}_{\mathrm{f}} \, \mathrm{d}\Omega^c, \tag{D.29}$$

$$\mathbf{C}^{\mathrm{pp},e} = \int_{\Omega^c} \mathbf{N}_{\mathrm{p}}^{\mathrm{T}} \mathbf{N}_{\mathrm{p}} \, \mathrm{d}\Omega^c. \tag{D.30}$$

ACKNOWLEDGEMENTS

FJV gratefully acknowledges the University of Colorado CRCW Seed Grant and NSF grant number CMMI-0900607 in support of this research.

REFERENCES

1. Baxter SC, Morales MO, Goldsmith EC. Adaptive changes in cardiac fibroblast morphology and collagen organization as a result of mechanical environment. *Cell Biochemistry and Biophysics* 2008; **51**:33–44.
2. Fernandez P, Bausch A. The compaction of gels by cells: a case of collective mechanical activity. *Integrative Biology* 2009; **1**:252–259.
3. Freyman TM, Yannas IV, Pek Y-S, Yokoo R, Gibson LJ. Fibroblast contraction of a collagen-gag matrix. *Biomaterials* 2001; **22**:2883–2891.
4. Ohsumi TK, Flaherty JE, Evans M, Barocas V. Three-dimensional simulation of anisotropic cell-driven collagen gel compaction. *Biomechanics and Modeling in Mechanobiology* 2008; **7**:53–62.
5. Wang J, Jia F, Gilbert T, Woo S. Cell orientation determines the alignment of cell-produced collagenous matrix. *Journal of Biomechanics* 2003; **36**(1):97–102.
6. Grinnel F, Lamke C. Reorganization of hydrated collagen lattices by human skin fibroblasts. *Journal of Cell Science* 1984; **66**:51–63.
7. Costa K, Lee E, Holmes J. Creating alignment and anisotropy and engineering heart tissue: role of boundary conditions in a model three-dimensional culture system. *Tissue Engineering* 2003; **9**(4):567–577.

17. Qiua J, Tanga T, Zhanga M, Zhuang Z. 2-D finite element simulation of cell–substrate debonding during cyclic stretch. *Tsinghua Science and Technology* 2009; **14**(2):27–31.
18. Yamada H, Mouri N, Nobuhara S. Three-dimensional morphometry of single endothelial cells with substrate stretching and image-based finite element modeling. *EURASIP Journal on Advances in Signal Processing* 2010; **2010**:Article ID 616091, 10 pages.
19. Wong HC, Tang WC. Finite element analysis of the effects of focal adhesion mechanical properties and substrate stiffness on cell migration. *Journal of Biomechanics* 2011; **44**(6):1046–1050.
20. Dolbow J, Möes N, Belytschko T. An extended finite element method for modeling crack growth with frictional contact. *Computer Methods in Applied Mechanics and Engineering* 2001; **190**(51–52):6825–6846.
21. Möes N, Cloirec M, Cartraud P, Remacle JF. A computational approach to handle complex microstructure geometries. *Computer Methods in Applied Mechanics and Engineering* 2003; **192**:3163–3177.
22. Belytschko T, Parimi C, Möes N, Sukumar N, Usui S. Structured extended finite element methods for solids defined by implicit surfaces. *International Journal for Numerical Methods in Engineering* 2003; **56**(4):609–635.
23. Dzyubachyk O, van Cappellen WA, Essers J, Niessen WJ, Meijering E. Advanced level-set-based cell tracking in time-lapse fluorescence microscopy. *IEEE Transactions on Medical Imaging* 2010; **29**(3):825–867.
24. Duddu R, Bordas S, Chopp D, Moran B. A combined extended finite element and level set method for biofilm growth. *International Journal for Numerical Methods in Engineering* 2008; **74**:848–870.
25. Coughlin MF, Stamenovic D. A prestressed cable network model of the adherent cell cytoskeleton. *Biophysics Journal* 2003; **84**:1328–1336.
26. Deshpande VS, McMeeking RM, Evans AG. A bio-chemo-mechanical model for cell contractility. *Proceedings of the National Academy of Science* 2006; **103**(38):14015–14020.
27. Walcott S, Sun SX. A mechanical model of actin stress fiber formation and substrate elasticity sensing in adherent cells. *Proceedings of the National Academy of Science* 2010; **107**(17):7757–7762.
28. Wang N, Butler JP, Ingber DE. Mechanotransduction across the cell surface and through the cytoskeleton. *Science* 1993; **260**:1124–1127.
29. Choquet D, Felsenfeld DF, Sheetz MP. Extracellular matrix rigidity causes strengthening of integrin–cytoskeletal linkages. *Cell* 1997; **88**:39–48.
30. Lecuit T, Lenne PF. Cell surface mechanics and the control of cell shape, tissue patterns and morphogenesis. *Nature Reviews Molecular Cell Biology* 2007; **8**:633–644.
31. Karcher H, Lammerding J, Huang H, Lee RT, Kamm RD, Kaazempur-Mofrad MR. A three-dimensional viscoelastic model for cell deformation with experimental verification. *Biophysics Journal* 2003; **85**

48. Yvonnet J, Quang HL, He QC. An XFEM/level set approach to modelling surface/interface effects and to computing the size-dependent effective properties of nanocomposites. *Computational Mechanics* 2008; **42**:119–131.
49. Farsad M, Vernerey FJ, Park HS. An extended finite element/level set method to study surface effects on the mechanical behavior and properties of nanomaterials. *International Journal for Numerical Methods in Engineering* 2010; **84**(12):1466–1489.
50. Mohammadi S. *Extended Finite Element Method*